An Objective Model for Identifying Secondary Eyewall Formation in Hurricanes

JAMES P. KOSSIN AND MATTHEW SITKOWSKI

Cooperative Institute for Meteorological Satellite Studies, University of Wisconsin—Madison, Madison, Wisconsin

(Manuscript submitted 26 June 2008, in final form 21 August 2008)

ABSTRACT

Hurricanes, and particularly major hurricanes, will often organize a secondary eyewall at some distance around the primary eyewall. These events have been associated with marked changes in the intensity and structure of the inner core, such as large and rapid deviations of the maximum wind and significant broadening of the surface wind field. While the consequences of rapidly fluctuating peak wind speeds are of great importance, the broadening of the overall wind field also has particularly dangerous consequences in terms of increased storm surge and wind damage extent during landfall events. Despite the importance of secondary eyewall formation in hurricane forecasting, there is presently no objective guidance to diagnose or forecast these events. Here a new empirical model is introduced that will provide forecasters with a probability of imminent secondary eyewall formation. The model is based on environmental and geostationary satellite features applied to a naïve Bayes probabilistic model and classification scheme. In independent testing, the algorithm performs skillfully against a defined climatology.

1. Introduction

The formation of a secondary eyewall in a tropical cyclone was described more than 50 years ago by Fortner (1958) for the case of Typhoon Sarah (1956). Secondary eyewalls are generally identified as quasi-circular rings of convective cloud at some distance outward from, and roughly concentric with, the primary eyewall of a hurricane (Fig. 1). Secondary wind maxima are often, but not always, collocated with the convective ring (Samsury and Zipser 1995), analogous to the collocation of the peak winds in a hurricane and the convection in the primary eyewall. The seminal work by Willoughby et al. (1982) explored the axisymmetric physics of secondary eyewall formation and the replacement of the primary eyewall by a contraction of the secondary eyewall that often follows its formation. The process of secondary eyewall formation and contraction, and the replacement of the primary eyewall by the secondary eyewall is typically referred to as an eyewall replacement cycle or a concentric eyewall cycle. Observational, theoretical, and numerical modeling studies have uncovered details of the dynamics associated with the presence of a primary and secondary eyewall and the ''moat'' region between them (Shapiro and Willoughby 1982; Black and Willoughby 1992; Dodge et al. 1999; Kossin et al. 2000; Camp and Montgomery 2001; Zhu et al. 2004; Wu et al. 2006; Terwey and Montgomery 2006; Rozoff et al. 2006, 2008; Houze et al. 2007; Wang 2008). With steady improvements to tropical cyclone monitoring, particularly with satellite-based microwave imagers, it has become clear that the formation of secondary eyewalls is not at all uncommon (e.g., Hawkins et al. 2006).

The motivation to understand and ultimately predict secondary eyewall formation and eyewall replacement events is high, as these events can have very serious consequences, particularly when they occur just prior to landfall. At great cost to life and property, Hurricane Andrew (1992) unexpectedly strengthened to a Saffir–Simpson category 5 hurricane while making landfall in southeastern Florida immediately following an eyewall replacement event (Willoughby and Black 1996; Landsea et al. 2004). Less immediately tangible, but perhaps more minatory, is the effect that secondary eyewall formation occurring away from land can have on the extent of the hurricane wind field. The local outer wind maxima often associated with the secondary eyewall can cause a rapid broadening of the overall wind field, and this can have profound effects on the

Corresponding author address: James P. Kossin, Cooperative Institute for Meteorological Satellite Studies, University of Wisconsin—Madison, Madison, WI 53706.
E-mail: kossin@ssec.wisc.edu

DOI: 10.1175/2008MWR2701.1

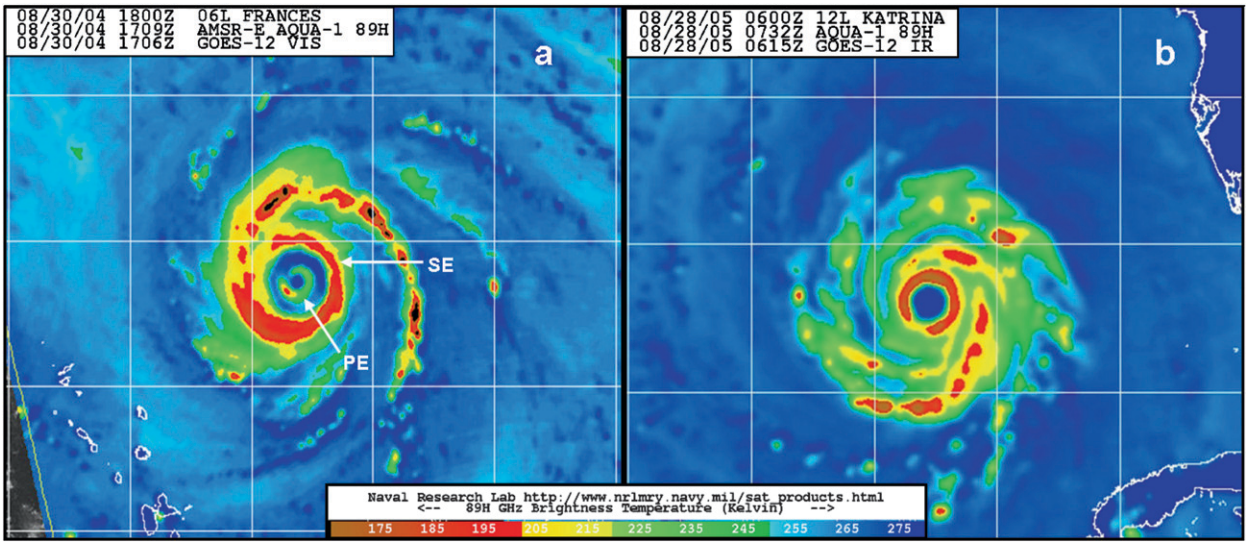

FIG. 1. Satellite microwave images of (a) Hurricane Frances on 30 Sep 2004, and (b) Hurricane Katrina on 28 Aug 2005. At the time of the image, convection in the primary eyewall (marked PE) is weakening while convection in the secondary eyewall (marked SE) strengthens, which is indicative that an ''eyewall replacement'' is underway. The warm (blue) ring between the primary and secondary eyewalls identifies the moat, which is associated with warm and dry subsiding air. In this case, the secondary eyewall continued to contract and ultimately replaced the primary eyewall. For comparison, Hurricane Katrina exhibits a single (primary) eyewall at the time of the image.

magnitude of the storm surge due to increased wind fetch. One of the most damaging direct effects of Hurricane Katrina (2005) was the storm surge resulting from the unusually broad region of significant winds surrounding the eye. For comparison, the storm surge associated with the landfall of very small and compact Hurricane Charley (2004) was much less damaging despite having much greater peak winds than Katrina at landfall.

A complete description of the physics responsible for initiating secondary eyewall formation has not yet been established. Internal dynamics in the form of outward propagating vortex Rossby waves may play a role (Montgomery and Kallenbach 1997), and asymmetries in the environment may also contribute to secondary eyewall formation through axisymmetrization processes (Kuo et al. 2004). Nong and Emanuel (2003) argue that secondary eyewall formation requires some external forcing from the ambient environment of the storm, and that once initiated, the survival of the nascent outer eyewall further depends on the ambient environmental conditions. Molinari and Vollaro (1989) suggest that secondary eyewall formation in Hurricane Elena (1984) might have been forced by interactions with upper-level momentum sources in the environment that the storm was moving into. Terwey and Montgomery (2006) argue that secondary eyewall formation can be initiated in a steady and homogeneous environment in the absence of a coherent external forcing. In this case, the environment may still modulate secondary eyewall formation, but without the presence of asymmetries, and without the occurrence of temporal changes.

Here, we will consider the observed environmental conditions that are associated with the formation of secondary eyewalls, and we will utilize this information to construct a diagnostic/predictive algorithm based on a Bayesian probabilistic model. We assume that internal dynamics such as Rossby wave forcing and axisymmetrization processes occur quasi-uniformly via convective forcing in the primary eyewall, and the ambient hurricane environment then modulates whether this forcing is realized in the initiation of a secondary eyewall. We will utilize the environmental parameters of the Statistical Hurricane Intensity Prediction Scheme (SHIPS; DeMaria and Kaplan 1994, 1999), which generally describe the mean axisymmetric environmental conditions centered on each hurricane, and we will consider additional information extracted from geostationary infrared satellite signatures around hurricanes. Our results suggest that these mean conditions do contain measurably useful information for diagnosing secondary eyewall formation.

2. Data and method

The first step for this project was the construction of a secondary eyewall formation database through a visual analysis of over 4500 microwave satellite images

covering the period 1997–2006 in all Northern Hemisphere tropical cyclone basins (available at the Web site of the Naval Research Laboratory in Monterey, California). Microwave instruments are able to see through the upper-level cirrus cloud that masks the presence of secondary convective rings in infrared images of hurricanes. The microwave imagery was used to examine nearly 175 tropical cyclones. Whenever possible, additional information from official forecast discussions, aircraft reconnaissance data and ''vortex messages,'' and both airborne and land-based radar data were also utilized.

There is presently no formal objective definition of what constitutes a secondary eyewall formation event. When a secondary eyewall was not explicitly identified in an aircraft vortex message or in a forecast statement, our identification of these events was based on a subjective assessment, using satellite microwave or radar imagery, of how circularly symmetric the outer convective features were. For example, a quasi-circular outer ring of convection that was clearly separated from the primary eyewall was required. This ring was also required to be roughly ''closed,'' that is, the convection had to form at least 75% of a complete circle. Additionally, we looked for cases where the moat region outside of the primary eyewall was clear of cloud and was evolving toward warmer microwave brightness temperatures. This warming in the moat signals an increase in local subsidence (Black and Willoughby 1992; Dodge et al. 1999; Houze et al. 2007) that is likely caused by an increase in inertial stability associated with the formation of a secondary wind maximum, which radially constrains the upper-level outflow from the primary eyewall (Rozoff et al. 2008). A typical signature in the microwave imagery of a hurricane with a primary and secondary eyewall and a well-defined moat is shown in Fig. 1a. It should be noted that the subjectivity inherent in the procedure described here introduces potential for misclassification errors in the new database. That is, a case where no secondary eyewall formed may mistakenly be classified as a secondary eyewall event, and vice versa. These errors can affect the interpretation of measures of model skill (Briggs et al. 2005), but it is beyond the scope of this paper to attempt to quantify this. We will assume that our database represents ground truth, although this is almost certainly not the case.

Because secondary eyewall formation has never been observed in a tropical storm or over land, we only consider hurricanes centered over water in this study (cf. Hawkins and Helveston 2004; Hawkins et al. 2006). Given the highly variable temporal sampling of satellite microwave and aircraft data, and the absence of any formal objective definition of what specifically constitutes a secondary eyewall formation event, determining the exact time of secondary eyewall formation is not a realistic expectation. Here we have simply attempted to identify when these events are ''imminent,'' which in our case means that a secondary eyewall formed at some time in the following 12 h. In addition to identifying secondary eyewall formation, it was also necessary to identify cases where secondary eyewall formation did not occur, defined as cases where no secondary eyewall formed in the following 12 h. There is one exception to this dichotomous event definition: cases within 12 h subsequent to secondary eyewall formation are not counted. This is based on the observation that secondary eyewall formation can occur repeatedly, but we found no instances where these events occurred within less than 12 h of each other (see, also, Willoughby et al. 1982).

Our secondary eyewall formation database includes tropical cyclones from all ocean basins in the Northern Hemisphere, but here we limit our attention to North Atlantic and central and eastern North Pacific hurricanes. This allows us to exploit the existing developmental dataset constructed for the Statistical Hurricane Intensity Prediction Scheme (DeMaria and Kaplan 1994, 1999). The SHIPS dataset contains information about the environment surrounding tropical cyclones in the North Atlantic and central and eastern North Pacific. Additionally, the SHIPS dataset contains information about the infrared satellite presentation of the storms deduced from Geostationary Operational Environmental Satellites (GOES; DeMaria et al. 2005). The SHIPS features are available every 6 h during the lifetime of each storm. Because of the marked differences in the environments and storm behaviors between the North Atlantic and central and eastern North Pacific basins, we will construct a separate algorithm for each.

The secondary eyewall formation database constructed for the North Atlantic contains 135 six-hourly data points (often referred to as ''fixes'') in which secondary eyewall formation occurred at some time in the following 12 h. There were 45 unique secondary eyewall events observed in the 10-yr period, and each event was estimated to occur within a period comprising three fixes at times t , $t + 6$ h, and $t + 12$ h. Similarly, there were 1010 fixes at hurricane intensity and over water, but no secondary eyewall formed in the following 12 h. In the central and eastern North Pacific, there are 42 fixes (14 unique events) in which secondary eyewall formation occurred at some time in the following 12 h, and 849 fixes at hurricane intensity and over water, but no secondary eyewall formed in the following 12 h. A much more detailed discussion of the general

climatology of secondary eyewall formation follows in section 3.

The new algorithm is based on application of the SHIPS features using a ''naïve Bayes'' probabilistic model and classifier (Zhang 2006; Domingos and Pazzani 1997). The model provides a conditional probability of class membership that depends on a set of measurable features. In our case, we have two classes representing the occurrence or absence of secondary eyewall formation. We denote these two classes as C_{yes} and C_{no}, respectively. The set of features is expressed as a vector $\mathbf{F}$ of length N (i.e., N is the number of features in the set). Using Bayes' theorem,[1] the probability of secondary eyewall formation conditional on the features $\mathbf{F}$ (or, equivalently, the probability of secondary eyewall formation when a particular set of features $\mathbf{F}$ is observed) can be described by

$$P(C_{\text{yes}}|\mathbf{F}) = \frac{P(C_{\text{yes}})P(\mathbf{F}|C_{\text{yes}})}{P(\mathbf{F})}. \quad (1)$$

The output of the model, $P(C_{\text{yes}} \mid \mathbf{F})$, is typically referred to as the ''posterior probability.'' The ''prior probability'' $P(C_{\text{yes}})$ is the probability that would be assigned if we had no measurements of the features. We define this as our climatology, and base it on the number of C_{yes} and C_{no} cases in a sample. Specifically, $P(C_{\text{yes}})$ is simply the number of C_{yes} cases divided by the total number of cases ($C_{\text{yes}} + C_{\text{no}}$). As an example, we find that $P(C_{\text{yes}}) \approx 0.12$ in the North Atlantic. If we had no other information, we would simply always assign a 12% probability that secondary eyewall formation will occur in the next 12 h whenever a hurricane is over water. In a pure ''yes or no'' classification scheme, a forecaster would then never predict secondary eyewall formation in the North Atlantic since the probability is always less than 50%. It is this defined climatology that our algorithm must out-perform in order to be skillful.

The likelihood of observing the feature set $\mathbf{F}$ when secondary eyewall formation is imminent is described by the factor $P(\mathbf{F} \mid C_{\text{yes}})$ in Eq. (1). This is referred to as a ''class-conditional probability.'' For comparison, the factor $P(\mathbf{F})$ in Eq. (1) gives the probability of observing the set of features $\mathbf{F}$ regardless of class membership. Formulating the probability density functions that will provide values for the class-conditional probability $P(\mathbf{F} \mid C_{\text{yes}})$ and the analogous expression $P(\mathbf{F} \mid C_{\text{no}})$ constitutes the ''supervised learning'' (training or model fitting) part of the algorithm construction. Following standard notation, we denote these probability density functions in lower case as $p(\mathbf{F} \mid C_{\text{yes}})$ and $p(\mathbf{F} \mid C_{\text{no}})$. It should be noted that in addition to likely misclassification error, our database represents only a small sample, and this introduces uncertainty into the prior probabilities and class-conditional probabilities deduced from it. In this respect, our application of Eq. (1) more formally constitutes an empirical Bayes model.

The feature set $\mathbf{F}$ can be described as points in an N-dimensional space (e.g., a scatterplot when $N = 2$), and the probability density functions $p(\mathbf{F} \mid C_{\text{yes}})$ and $p(\mathbf{F} \mid C_{\text{no}})$ that need to be constructed are thus also N dimensional. Determining likelihoods of the points in this N-dimensional space can be performed using a variety of methods (e.g., K-nearest neighbor) but can become very computationally expensive, even when N is fairly small. For example, if the probability density function for each of the N features was resolved into 100 bins, then $p(\mathbf{F} \mid C_{\text{yes}})$ and $p(\mathbf{F} \mid C_{\text{no}})$ would each require 100^N bins. For a set of only six features, sampling each of the two probability density functions would then require 8 terabytes of computer memory if stored using double-precision values. This has been referred to as ''the curse of dimensionality'' (Bellman 1957).

An assumption that considerably reduces the dimensionality of the problem is that the features are independent within each class, so that $P(\mathbf{F} \mid C_{\text{yes}}) = \Pi_{i=1}^{N} P(F_i \mid C_{\text{yes}})$ where F_i represents a single feature of the set $\mathbf{F}$. In this case, Eq. (1) can be written as

$$P(C_{\text{yes}}|\mathbf{F}) = \frac{P(C_{\text{yes}})\Pi_{i=1}^{N} P(F_i|C_{\text{yes}})}{P(\mathbf{F})}. \quad (2)$$

Noting that $P(C_{\text{yes}} \mid \mathbf{F}) + P(C_{\text{no}} \mid \mathbf{F}) = 1$, the denominator of (2) can be written as

$$P(\mathbf{F}) = P(C_{\text{yes}})\Pi_{i=1}^{N} P(F_i|C_{\text{yes}}) + P(C_{\text{no}})\Pi_{i=1}^{N} P(F_i|C_{\text{no}}). \quad (3)$$

Equations (2) and (3) reduce the model described by Eq. (1) from an N-dimensional feature space to two sets of N one-dimensional probability density functions $p(F_i \mid C_{\text{yes}})$ and $p(F_i \mid C_{\text{no}})$. Now, if the probability density functions were resolved into 100 bins, then $p(F_i \mid C_{\text{yes}})$ and $p(F_i \mid C_{\text{no}})$ would each require $100N$ bins, versus 100^N bins. Revisiting the six-feature example above, the memory requirement for storing and sampling the probability density functions is reduced from 8 terabytes to 4.8 kilobytes.

The Bayes model is also easily reduced to a classifier by applying a decision rule to the model output. One simple decision rule is to assign the class with the greatest posterior probability given by the model. In our

[1] Further detail on Bayes' theorem and a meteorological application can be found in Wilks (2006). There is also an excellent discussion in Bishop (1995) using an example of text classification.

binary ''yes or no'' classification problem, we would then simply choose the class with a probability greater than 50%. A slightly more complex procedure is to enforce some optimal decision threshold based on analysis of a receiver operating characteristic (ROC) diagram (see, e.g., Wilks 2006), but it is not always clear how to define an optimal threshold and will generally depend on the priorities of the model users. This will be discussed further in section 4.

The assumption that the features can be treated independently within each class constitutes the ''naïve'' aspect of the naïve Bayes classifier defined by Eqs. (2) and (3) combined with a decision rule. Despite this markedly simplifying assumption, the naïve Bayes classifier has been shown to perform as well and in some cases better than more sophisticated models in a variety of applications, even when the independence assumption is strongly violated (Domingos and Pazzani 1997; Hand and Yu 2001; Zhang 2006).

The features applied to the probabilistic model are chosen from the SHIPS dataset based on the following criteria: The feature must be significantly different, at greater than the 95% confidence level, between the secondary eyewall formation cases and the cases where no secondary eyewall formed. This was determined using a two-sided Student's t test. There were a number of features in the SHIPS dataset that satisfied this criterion, and these were then reduced to a final feature set. The final choice of features was based on the performance of the naïve Bayes model using a ''leave-one-season-out'' cross-validation technique. Since model performance metrics will typically exhibit significant interannual variability, this type of cross-validation provides a more robust indication of the expected long-term future performance of the model than validating on only one or two years. For each of the 10 years (1997–2006), we removed all data from that year, formed the prior probabilities [$P(C_{\text{yes}})$ and $P(C_{\text{no}})$] and the class-conditional probability density functions for each of the features [$p(F_i \mid C_{\text{yes}})$ and $p(F_i \mid C_{\text{no}})$] with the data from the remaining years, and then estimated posterior probabilities of secondary eyewall formation, using Eqs. (2) and (3), for the year that was removed. This was repeated for each year, and the probabilities for each year were subjoined to ultimately include all 10 years.

The class-conditional probability density functions, $p(F_i \mid C_{\text{yes}})$ and $p(F_i \mid C_{\text{no}})$, were constructed from the data for each feature using kernel-based estimation with a normal kernel function and a window parameter that results in a feature-sampling size of 100 bins. There was little sensitivity in cross-validated model performance when the number of bins was increased or decreased. The prior probabilities $P(C_{\text{yes}})$ and $P(C_{\text{no}})$ were also subjoined in the cross-validation procedure to be used later when the model is tested against climatology. The values remain constant through each year but change between years because they are based on the event counts of the remaining years in the leave-one-out process. In the North Atlantic the prior probabilities range from 9%–13% (the lowest occurs when the 2004 season is removed), and their mean is 12%. In the central and eastern North Pacific, they range from 4% to 6%, with a mean of 5%.

It should be noted that the class-conditional feature sets do exhibit serial correlation, which has the potential to inflate t test scores. The serial correlation results from having sequential 6-hourly SHIPS features within the 12-h window we use to define an imminent event, and from multiple sequential periods during nonevents. Formal correction for serial correlation is often problematic in statistical hurricane studies because individual hurricane time series are autoregressive but also independent of the other hurricane time series in the larger sample. Here, we note this caveat and consider our cross-validation of the algorithm to present an accurate representation of expected model performance. It is also somewhat reassuring that the separation of each feature applied to the North Atlantic and central and eastern North Pacific is significant at 99.9% confidence. Following the cross-validation criteria outlined in Elsner and Schmertmann (1994), the t tests for significant separation of the features by class were then repeated with each year omitted from the data. This was done to be sure that the choice of features was independent of data in the omitted year. We found no instances where significance fell below the 95% confidence threshold (none fell below the 99% threshold in the North Atlantic), and the set of features was accordingly held fixed in the cross-validation.

The cross-validated performance of the model was measured using a variety of metrics, which are outlined here. To assess the probabilistic model, we used the Brier skill score and the attributes diagram. The Brier skill score is defined as $1 - B/B_{\text{ref}}$, where

$$B = \frac{1}{k}\sum_{i=1}^{k}[P(C_{\text{yes}}|\mathbf{F})_i - O(i)]^2,$$

$$B_{\text{ref}} = \frac{1}{k}\sum_{i=1}^{k}[P(C_{\text{yes}}) - O(i)]^2,$$

and $O(i) = 1$ or 0 for cases of secondary eyewall formation or no formation, respectively. Here, k is the number of cases the algorithm is applied to, and $P(C_{\text{yes}} \mid \mathbf{F})_i$ is the posterior probability estimate deduced from Eq. (2) for a specific individual time. To assess the binary (yes/no)

TABLE 1. Number of North Atlantic (boldface) and Central and Eastern North Pacific hurricanes, major hurricanes, hurricanes that exhibited at least one secondary eyewall during their lifetime, and number of individual secondary eyewall formation (SEF) events from 1997 to 2006.

	1997	1998	1999	2000	2001	2002	2003	2004	2005	2006	Total
Hurricanes	**3**	**10**	**8**	**8**	**9**	**4**	**7**	**9**	**15**	**5**	**78**
	9	9	6	6	8	8	7	6	7	11	77
Major Hurricanes	**1**	**3**	**5**	**3**	**4**	**2**	**3**	**6**	**7**	**2**	**36**
	7	6	2	2	2	6	0	3	2	6	36
SEF Hurricanes	**2**	**3**	**2**	**1**	**3**	**2**	**2**	**5**	**5**	**1**	**26**
	2	2	0	0	2	2	0	0	0	4	12
SEF Events	**3**	**3**	**3**	**1**	**3**	**2**	**4**	**16**	**9**	**1**	**45**
	2	2	0	0	2	2	0	0	0	6	14

classification algorithm we considered metrics based on 2×2 contingency tables: the Peirce skill score, the ''probability of detection'' (or ''hit rate''), and the ''false alarm rate.'' The area under the Receiver Operating Characteristic curve was also used as an additional measure of the model's overall ability to distinguish secondary eyewall formation events from nonevents. All of these tools are described further in Wilks (2006).

One additional skill score (Briggs and Ruppert 2005) based on 2×2 contingency tables was also applied to assess model performance against climatology. The optimal yes/no predictions based naïvely on climatology would always indicate that no secondary eyewall formation is expected to occur. This would, for example, result in 88% correct predictions in the North Atlantic, and the model should improve on this in order to be considered skillful if the error (or loss) is considered to be symmetric. Here, symmetric loss indicates equal penalty for a false negative (miss) and false positive (false alarm). Note that this is markedly different from the Peirce skill score, which weakly penalizes false alarms and provides a measure of confidence to forecasters who must predict the occurrence of rare events. The Briggs and Ruppert skill score under the assumption of symmetric loss is given by

$$\hat{K} = \frac{n_{11} - n_{01}}{n_{11} + n_{10}},$$

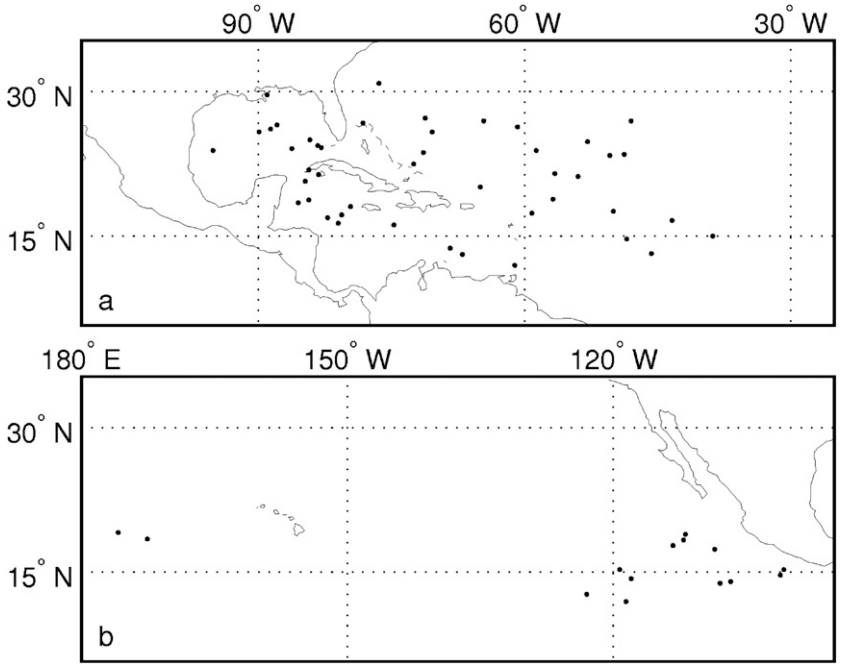

FIG. 2. Locations of secondary eyewall formation events in the (a) North Atlantic and (b) central and eastern North Pacific Oceans.

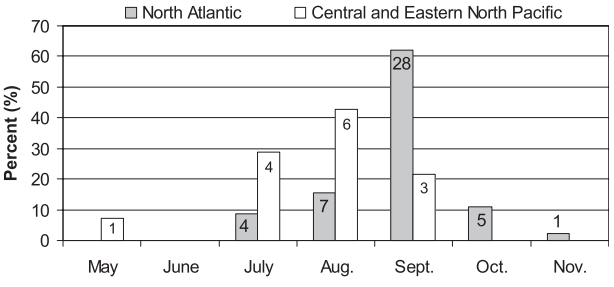

FIG. 3. Percent of total secondary eyewall formation events by month. Numbers indicate the number of secondary eyewall formation events per month. The shaded bars denote the North Atlantic and the unshaded bars denote the central and eastern North Pacific.

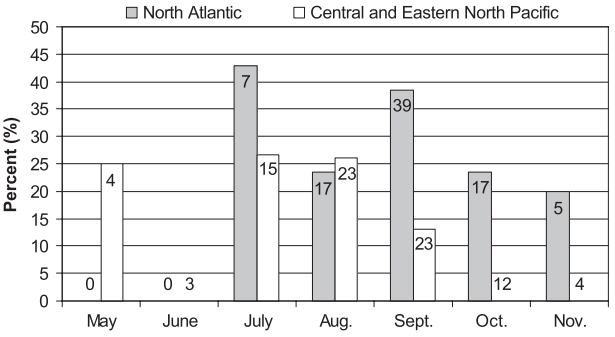

FIG. 4. Ratio (%) of the number of hurricanes, per month, that formed secondary eyewalls divided by the number of hurricanes per month. Numbers indicate the number of hurricanes per month. Hurricanes that cross from one month to another are counted in both months.

where n_{11}, n_{01}, and n_{10} are the number of correct positive classifications (hits), false positive classifications (false alarms), and false negative classifications (misses), respectively. This skill score can be extended to account for asymmetric loss (e.g., situations where overprediction may be more or less costly than underprediction) and, as mentioned briefly above, for misclassification error (Briggs et al. 2005).

The SHIPS features used in the algorithm are a combination of storm-based variables such as current intensity and latitude, environmental variables such as vertical wind shear and middle- to upper-level relative humidity, and geostationary satellite infrared-based variables. In addition to the satellite-based features contained in the SHIPS dataset, we also considered satellite-based features constructed from a principal component analysis of storm-centered azimuthally averaged infrared brightness temperature profiles derived from the hurricane satellite (HURSAT) dataset available at the National Oceanic and Atmospheric Administration (NOAA) National Climatic Data Center (Knapp and Kossin 2007; Kossin et al. 2007a,b). The eigenmodes of the analysis describe varying radial structures of the average storm-centered brightness temperature, and the expansion coefficients associated with the eigenmodes were considered as potential features. We found that the expansion coefficient associated with the radial structure described by the fourth leading eigenmode was most useful in separating between our two classes. This was the case in both the North Atlantic and central and eastern North Pacific. This eigenmode explains only 2% of the azimuthally averaged brightness temperature variation (also true for both basins) but was found to consistently improve model performance in both ocean basins. The radial structure of this eigenmode (not shown) has a local amplitude maximum beyond ~100 km from hurricane center and may be capturing anomalous subsidence warming of the upper-level cirrus shield in this region. This may be related to increased inertial stability caused by local acceleration of the tangential wind often associated with a secondary eyewall (Rozoff et al. 2008), but this relationship between brightness temperature and storm dynamics is uncertain.

3. Secondary eyewall formation climatology

a. North Atlantic climatology

For this study, a total of 45 secondary eyewall formation events were documented in 26 North Atlantic hurricanes[2] during the 10-yr period 1997–2006. Here, an event is described by the occurrence of secondary eyewall formation, but there is no guarantee that these events are always followed by a complete concentric eyewall cycle. The period 1997–2006 was chosen based on the availability of satellite microwave imagery. Since the goal of the study is to identify unique or anomalous characteristics associated with secondary eyewall formation events relative to the larger sample of nonevents, it was important to not just identify secondary eyewall formation, but also to correctly identify when formation did not occur. To make such assessments, a more comprehensive coverage is required but is not provided by infrared satellite instruments, which cannot identify convective structures beneath the ubiquitous cirrus cloud over hurricanes, or sparse in situ measurements.

The occurrence of secondary eyewall formation events by year is shown in Table 1. At least one event was observed during each year in the period, and one-third

[2] The climatology for the central and eastern North Pacific region will be discussed in section 3b.

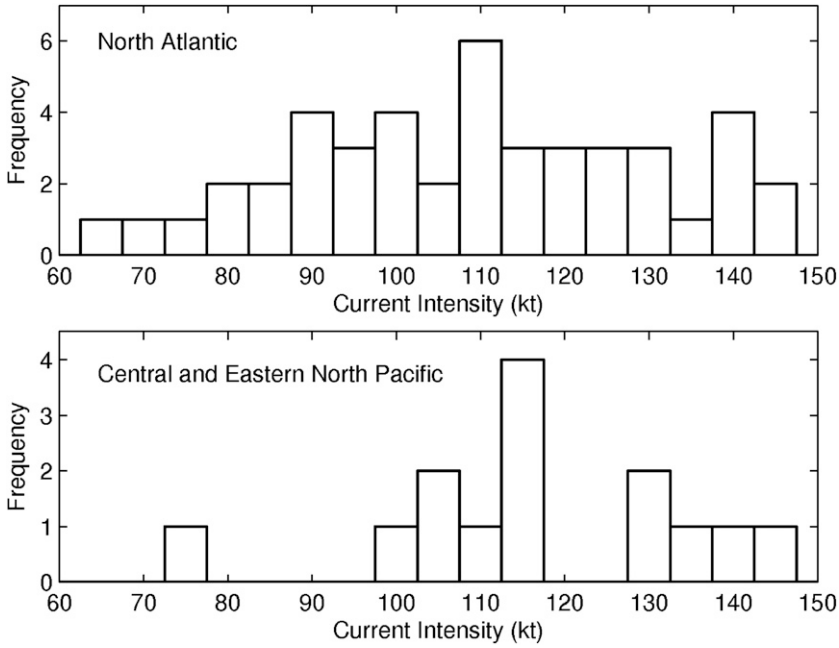

FIG. 5. Frequency of secondary eyewall formation events binned by mean current intensity during the time period of the event. There are a total of 45 observed events in the North Atlantic and 14 in the central and eastern North Pacific.

of all hurricanes developed a secondary eyewall at least once during their lifetime. Comparatively, 70% of major hurricanes (Saffir–Simpson category 3–5) were observed to form secondary eyewalls at least once during their lifetimes. The high number of individual events in 2004 is largely due to the multiple-formation events observed in Hurricanes Ivan and Frances, both of which were long-lived Cape Verde systems (six unique events were observed in Hurricane Ivan and four events were observed in Hurricane Frances). All secondary eyewall formation events were observed to occur in a region bounded by 12°–31°N, 39°–95°W (Fig. 2), which includes the Caribbean Sea and Gulf of Mexico. Secondary eyewall formation is observed to occur over open water and near large and small landmasses.

In the period 1997–2006, secondary eyewalls were observed to form during each month of the hurricane season except June, while more than 60% of the total number were observed during September (Fig. 3). When the number of hurricanes per month that formed secondary eyewalls is normalized by the number of hurricanes per month, the percentage of hurricanes that form secondary eyewalls ranges from about 20% in November to about 43% in July and 38% in September (Fig. 4). That is, a hurricane is apparently more likely to form a secondary eyewall in July or September than in other months. If the maximum intensity that each hurricane achieves in its lifetime is considered by month, we find that the mean of these maximum lifetime intensities is lower in July (~89 kt, 46 m s^{-1}) than in August, September, and October (~100 kt, 51 m s^{-1}), which is suggestive that the environmental conditions in July are more favorable for secondary eyewall formation but not necessarily for achieving high intensities relative to other months. The small sample size in July (only seven hurricanes and three that formed a secondary eyewall over the 10-yr period), however, may not be representative of the larger population that we are sampling from, and the meaning of the relatively high percentage of hurricanes that form secondary eyewalls in July should be considered with caution.

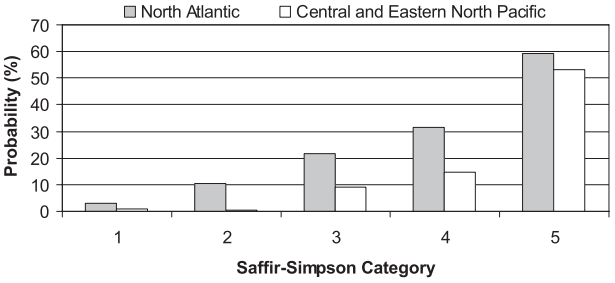

FIG. 6. Climatological probability, based on counts, of secondary eyewall formation as a function of current intensity (grouped by Saffir–Simpson category). The values reflect the climatological probability, for any time that a hurricane is over water, that secondary eyewall formation is imminent.

TABLE 2. SHIPS features applied to the Bayes probabilistic model in the North Atlantic.

SHIPS feature	Description	Preference for secondary eyewall formation
VMX	Current intensity	Stronger
LAT	Latitude	Further south
D26C	Climatological depth of 26°C ocean isotherm	Deeper
U200	200-hPa zonal wind (200–800 km from center)	Weaker (near zero), very narrow range
RHHI	500–300-hPa relative humidity	Moister
TWAC	0–600-km average symmetric tangential wind at 850 hPa from NCEP analysis	Stronger
PENC	Azimuthally averaged surface pressure at outer edge of vortex	Lower
SHRD	850–200-hPa shear magnitude	Weaker, narrow range
VMPI	Maximum potential intensity	Higher, very narrow range
IR00–05	Standard deviation (from axisymmetry) of GOES infrared brightness temperature between 100 and 300 km	Smaller (more axisymmetric)
IR00–16	Average GOES infrared brightness temperature between 20 and 120 km	Colder, narrow range

Secondary eyewalls were observed to form within a broad range of hurricane intensities (Fig. 5). The average intensity during an event was 109 kt (56 m s^{-1}), which denotes a strong Saffir–Simpson category 3 hurricane. It is generally understood that the current intensity of a hurricane is a controlling factor in the probability of secondary eyewall formation, with higher probability associated with stronger hurricanes. Figure 6 provides a rough quantification of this relationship within the limitations of our data sample. Here we considered the probability that a secondary eyewall will form in the following 12 h, so that the values in Fig. 6 are equivalent to recasting the prior probability [denoted $P(C_{\text{yes}})$ in section 2] as a function of hurricane intensity. We find that the probability of imminent secondary eyewall formation at any time during category 5 status is about 60%, so that it is more likely than not that an event is about to occur (if an event is not already underway). This probability is reduced to about 30% for category 4 hurricanes, 20% for category 3 hurricanes, 10% for category 2 hurricanes, and is less than 5% for category 1 hurricanes.

Another essential factor in the climatology of secondary eyewall formation is the description of the characteristics of intensity change associated with these events. Willoughby et al. (1982) documented intensity evolution for a few case studies, and the present paradigm describes a weakening associated with secondary eyewall formation, often followed by a reintensification as the secondary eyewall contracts. These intensity deviations are generally observed to be transient and occur on intradaily time scales. Consequently, the archival records of hurricane intensity comprising the 6-hourly ''best track'' fixes are not particularly well suited for the task since the best track is a temporally smoothed record by design. This was corroborated with our secondary eyewall formation database, as we found that the statistics of best-track intensity change associated with secondary eyewall formation were not distinguishable from the larger sample of hurricanes. This result remained robust when we only considered best-track fixes that were contemporaneous with aircraft reconnaissance measurements. There is a need, then, for a future study that exploits the present large archive of raw high temporal resolution aircraft reconnaissance data to form a more exhaustive and modern climatology of intensity evolution associated with secondary eyewall formation, but this is not attempted here.

TABLE 3. Four 2 × 2 contingency tables for classification of secondary eyewall formation events in the North Atlantic. The top 2 × 2 table is based on the climatological probability of secondary eyewall formation. The next table is based on the probability estimated from our new algorithm using current intensity as the sole feature. The next table shows how the inclusion of the SHIPS environmental features improves the algorithm performance. The bottom table is based on the addition of the GOES satellite-derived features. All values are based on cross-validation of the model.

		Observed	
	Forecast	Yes	No
Climatology	Yes	0 (hits)	0 (false alarms)
	No	129 (misses)	936 (correct negatives)
Current intensity only	Yes	17	15
	No	112	921
Current intensity plus SHIPS environmental	Yes	29	20
	No	100	916
Current intensity plus SHIPS environmental plus GOES	Yes	39	21
	No	90	915

TABLE 4. Performance metrics of the model applied to the North Atlantic.

	Brier skill score	Peirce skill score	Briggs and Ruppert skill score	Probability of detection	False alarm rate	Area under ROC curve
Climatology	0%	0%	0%	0%	0%	0.50
Current intensity only	12%	12%	2%	13%	2%	0.77
Current intensity plus SHIPS environmental	18%	20%	7%	22%	2%	0.86
Current intensity plus SHIPS environmental plus GOES	21%	28%	14%	30%	2%	0.86

b. Central and eastern North Pacific climatology

A total of 14 secondary eyewall formation events were observed in 12 hurricanes from 1997 to 2006, or roughly one-third of the events observed in the North Atlantic (Table 1). The number of hurricanes and major hurricanes is roughly the same in both basins during this period. About 16% of the hurricanes and 33% of the major hurricanes were observed to form a secondary eyewall at some time. The majority of formation events occurred near the west coast of Mexico, east of 125°W longitude (Fig. 2), which is within the region of highest track density in the broader climatology of eastern North Pacific hurricanes. Hurricane Ioke (2006) was the only hurricane observed to form a secondary eyewall in the central North Pacific. More secondary eyewall events (43%) occur during August than other months (Fig. 3). Although no events were observed in June, there was a single event observed in May in Hurricane Adolph (2001). When the number of secondary eyewall formation events per month is normalized by the total number of hurricanes per month, the percentage of hurricanes that form secondary eyewalls is lower or roughly equivalent compared to the North Atlantic during the more active months (Fig. 4). The percentage of hurricanes that formed secondary eyewalls in the central and eastern North Pacific is roughly equivalent during May, July, and August, but it is not clear whether the high percentage in May is physical or due to sampling issues in our limited dataset (only four hurricanes were observed). The average intensity around the time of secondary eyewall formation was 117 kt (60 m s^{-1}), which describes a category 4 hurricane (Fig. 5).

4. Application and performance characteristics of the probabilistic model

a. Application to the North Atlantic

The feature set applied in the North Atlantic comprises nine storm/environmental features and two satellite-based features from the SHIPS dataset (described in Table 2) plus the additional satellite-derived feature derived from the principal component analysis described at the end of section 2. We find that secondary eyewall formation is associated with higher maximum potential intensity[3] (VMPI), lower vertical wind shear (SHRD), weaker upper-level zonal winds (U200), a deep layer of underlying warm water (D26C), and higher middle- to upper-level relative humidity (RHHI). The relationship with higher relative humidity agrees well with the numerical findings of Nong and Emanuel (2003), and with the basic idea that organized convection in the tropics is sensitive to humidity and dry air entrainment above the boundary layer (e.g., Ooyama 1969). The higher MPI suggests that secondary eyewall formation is favored in an environment that is more thermodynamically supportive of persistent deep convection. In typical tangential wind fields in hurricanes, the radial gradient of angular velocity will inherently tend to organize asymmetric convection into a circular ring. The sensitivity of secondary eyewall formation to shear may be an indication that the shear disrupts this symmetrization process, although the relationship between convection and shear is significantly more complicated (e.g., Kwon and Frank 2008). The class-separation of the 200-hPa zonal wind suggests that secondary eyewall formation prefers quiescent upper levels. The upper-level wind is correlated with the shear ($r = 0.7$), but it is included because it contains additional independent information specifically about the upper levels and was found to lower the false alarm rate of the model. The colder and more axisymmetric GOES brightness temperature fields are also reconcilable with the preference for stronger storms in a low-shear environment to form secondary eyewalls. The physical mechanisms underlying the statistical relationships uncovered here are of great interest, and are presently being explored in theoretical and numerical modeling frameworks, but our purpose here is to exploit these relationships to

[3] In the SHIPS developmental dataset, maximum potential intensity is calculated as described in Bister and Emanuel (1998).

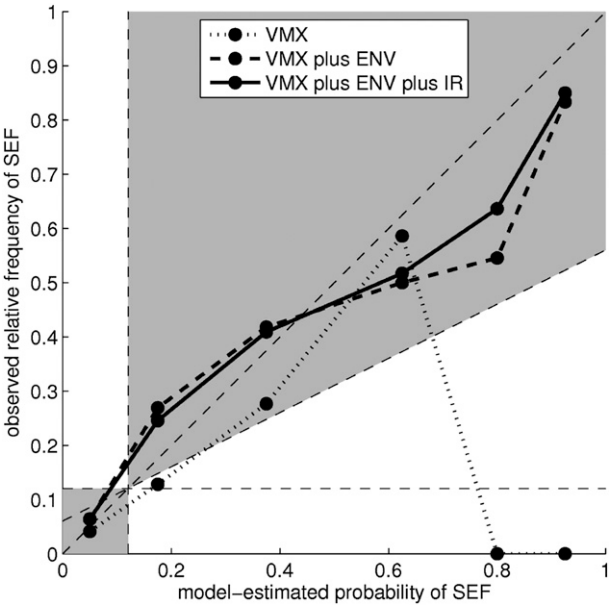

FIG. 7. Attributes diagram for the Bayes probabilistic model for three different choices of features: current intensity only (VMX), current intensity plus SHIPS environmental features (VMX plus ENV), and current intensity plus SHIPS environmental features plus infrared-based features (VMX plus ENV plus IR). SEF is shorthand for secondary eyewall formation. The posterior probabilities given by the model were placed in six bins of varying ranges with each point plotted at the bin center. The bin ranges were chosen ad hoc to reduce sampling fluctuations. The counts within each bin, from least to greatest probability, are {585, 242, 206, 29, 1, 2} for VMX only, {883, 78, 55, 26, 11, 12} for VMX plus ENV, and {904, 57, 44, 29, 11, 20} for VMX plus ENV plus IR.

construct an algorithm that may be usefully applied operationally.

An important point to emphasize is that we use current intensity (VMX in Table 2) as a feature in the Bayes probabilistic model, which represents a strong violation of the assumption of feature independence required for the ''naïve approximation'' of the model. For example, it is well known that current intensity is closely related to ambient vertical wind shear. As noted in section 2, the model has been shown to typically perform very well regardless of this violation, but the inclusion of current intensity makes it more difficult to explicitly separate the effect of storm intensity versus storm environment on secondary eyewall formation. To mitigate this, we will compare model performance for three cases: 1) using current intensity as the only feature, 2) using current intensity and the SHIPS environmental features, and 3) using current intensity, SHIPS environmental features, and satellite-derived features.

Utilizing the subjoined sets of prior and posterior probabilities formed with the cross-validation method described in section 2, the performance of the probabilistic model and classifier applied to the North Atlantic is shown in Tables 3 and 4.[4] In this case, the classifier is based on the maximum posterior probability decision rule; that is, we choose whichever class, C_{yes} or C_{no}, is assigned a probability greater than 50%. Since the prior probabilities (i.e., the climatological expectation based on counts) are always much smaller than 50%, there would never be a prediction of imminent secondary eyewall formation based on climatology. This is reflected in the 2×2 contingency table at the top of Table 3 and in the metrics in the top row of Table 4. When the current intensity is used as the sole feature in our model, we see a measurable increase in the probability of detection and in the skill as measured using the Brier and Peirce skill scores, but only a marginal increase in the Briggs and Ruppert skill score. The area under the ROC curve, which provides an overall measure of the model's ability to distinguish between classes, is 0.77. This value can range from 0.5 to 1.0 where 0.5 is the expectation based on climatology. In general, 0.5–0.6 is considered a failure of the model, 0.6–0.7 is poor, 0.7–0.8 is fair, 0.8–0.9 is good, and 0.9–1.0 is excellent, so here the model does a fair job of distinguishing between classes when current intensity is the sole input feature.

The attributes diagram for the model is shown in Fig. 7. The 45° diagonal line represents perfect reliability across the range of possible probabilities. Points that lie within the shaded region contribute to increasing model skill and points outside the region decrease skill [see Wilks (2006) for more detail if needed]. When current intensity is the sole feature, the model does a reasonable job of correctly assigning lower probabilities, as seen by the proximity of some of the points to the perfect reliability diagonal, but the model completely fails to correctly assign higher probabilities. When the SHIPS environmental features are included, the model improves markedly. This is seen clearly in the attributes diagram, which shows overall improvement with particularly good improvement in correctly assigning high probabilities of secondary eyewall formation. The Brier and Peirce and Briggs and Ruppert skill scores, probability of detection, and the area under the ROC curve all increase, while the false alarm rate remains relatively constant (Tables 3 and 4). When the GOES satellite-based features are added to the model, we see consistent improvement across the full range of probability esti-

[4] The numbers of 6-hourly fixes reflected in Table 3 (and also in Table 8 in section 4b) are slightly reduced from the numbers listed in section 2 because of missing fixes in the SHIPS dataset.

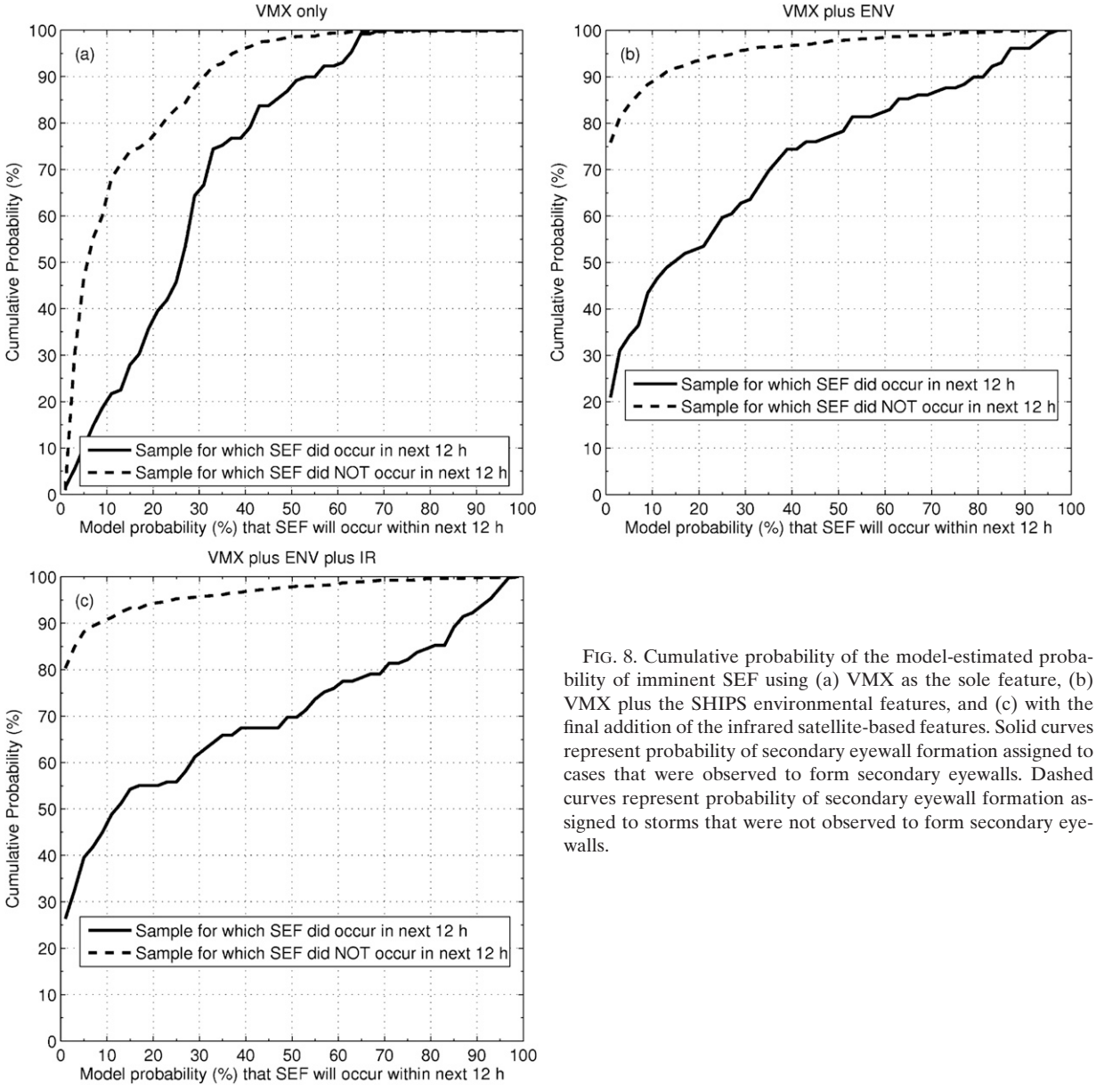

FIG. 8. Cumulative probability of the model-estimated probability of imminent SEF using (a) VMX as the sole feature, (b) VMX plus the SHIPS environmental features, and (c) with the final addition of the infrared satellite-based features. Solid curves represent probability of secondary eyewall formation assigned to cases that were observed to form secondary eyewalls. Dashed curves represent probability of secondary eyewall formation assigned to storms that were not observed to form secondary eyewalls.

mates, that is, all points move closer to perfect-reliability diagonal. The number of hits increases from 29 to 39, increasing the probability of detection from 20% to 28%, while the number of false alarms only slightly increases, from 20 to 21. Inclusion of the three GOES features increases the Brier and Peirce and Briggs and Ruppert skill scores from 18% to 21%, 20% to 28%, and 7% to 14%, respectively, and the area under the ROC curve suggests that the model is good at distinguishing between classes.

Figure 8 shows the cumulative distributions of the probabilities of secondary eyewall formation assigned by the model when separated by the observed class. When current intensity (VMX) alone is used (Fig. 8a), roughly 65% of the observed ''no-formation cases'' were assigned a probability of formation of less than 10%, while 80% of the observed formation cases were assigned a probability of more than 10%. Only about 12% of the formation cases were assigned a probability greater than 50% using VMX as the sole feature. When the SHIPS environmental features are added to the model (Fig. 8b), there is a large increase in the number of cases that are assigned a near-zero probability of secondary eyewall formation. Roughly 75% of the

TABLE 5. The 2 × 2 contingency tables for two different decision rules applied to the North Atlantic.

		Observed	
	Forecast	Yes	No
Decision rule: Posterior probability greater than prior probability	Yes	69	83
	No	60	853
Decision rule: Posterior probability greater than "optimal" threshold	Yes	97	186
	No	32	750

assigned probabilities were near zero for the cases of no observed formation, and about 20% of the observed formation cases were assigned a probability greater than 50%. When the GOES-based features are added (Fig. 8c), about 30% of the observed formation cases were assigned a probability greater than 50%, while about 25% were assigned a probability of formation near zero.

The contingency tables and the metrics derived from those tables—the probability of detection, false alarm rate, and Peirce and Briggs and Ruppert skill scores—shown in Tables 3 and 4 are based on a decision threshold of 50% probability. As discussed in section 2, this may not be an optimal threshold, but the choice of what should define optimal is generally situation-dependent. For example, in some situations, keeping the false alarm rate low may be a priority, while in others, maximizing the probability of detection may be of greater importance. The Bayes probabilistic model provides posterior probabilities, which can then be subjected to any decision rule to form a classification assignment. In an operational hurricane-forecasting environment, the model would most likely be used in the same manner that other models—empirical or numerical—are used. That is, the forecaster can assess the evolution of the probability of secondary eyewall formation in real time, and form an expert judgment based on a variety of available information and a working knowledge of the traits and behaviors of the models being considered. In this case, there is no need to reduce the information provided by the model by reducing it to a binary classifier, and the Peirce and Briggs and Ruppert skill scores based on the 2 × 2 contingency tables may be less relevant to the expected operational model performance than the Brier skill score, which is based on the actual continuum of probabilities produced by the model. Nonetheless, it is instructive to consider the performance of the classifier based on various decision rules, if for no other reason than to scrutinize the model characteristics as deeply as possible.

Here we consider two additional decision thresholds, given by the prior (climatological) probabilities and by an analysis of the ROC curve. For the latter, we chose the threshold defined by the point on the curve closest to the point (0, 1), which represents a perfect model in the ROC diagram and maximizes the Peirce skill score. Because of the large number of probabilities that are near zero, as discussed above, this threshold value is in fact very small (~2%). Table 5 shows the 2 × 2 contingency tables, based on the model using all features [VMX plus environmental (ENV) and infrared (IR)-based features], for the two different thresholds, and Table 6 shows the performance metrics based on the contingency tables. When the threshold is lowered, there is a marked increase in the probability of detection as well as skill, as measured by the Peirce skill score, but there is a commensurately large increase in the false alarm rate. The increase in false alarms results in a complete loss of skill as measured by the Briggs and Ruppert skill score. When the optimal threshold based on the ROC curve analysis is used, the number of false alarms increases by a factor of about 9 compared to Table 3, while the number of hits increases by a factor of about 2.5. The Peirce skill score increases to 55% while the Briggs and Ruppert skill score shows considerably less skill than climatology. This reemphasizes the challenge of objectively defining an optimal classifier; maximizing a particular skill score may not provide the best tool if low false alarm rates are as important as high probabilities of detection.

To provide a sense of the model characteristics when applied to individual hurricanes, Fig. 9 shows the evolution of the model-assigned probabilities of secondary eyewall formation in four North Atlantic hurricanes. The relationship between hurricane intensity and the probability of secondary eyewall formation is broadly evident, but it is also evident that other factors are

TABLE 6. Performance metrics of the model under two decision rules.

	Peirce skill score	Briggs and Ruppert skill score	Probability of detection	False alarm rate
Decision rule: Posterior probability greater than prior probability	45%	−11%	53%	9%
Decision rule: Posterior probability greater than "optimal" threshold	55%	−70%	75%	20%

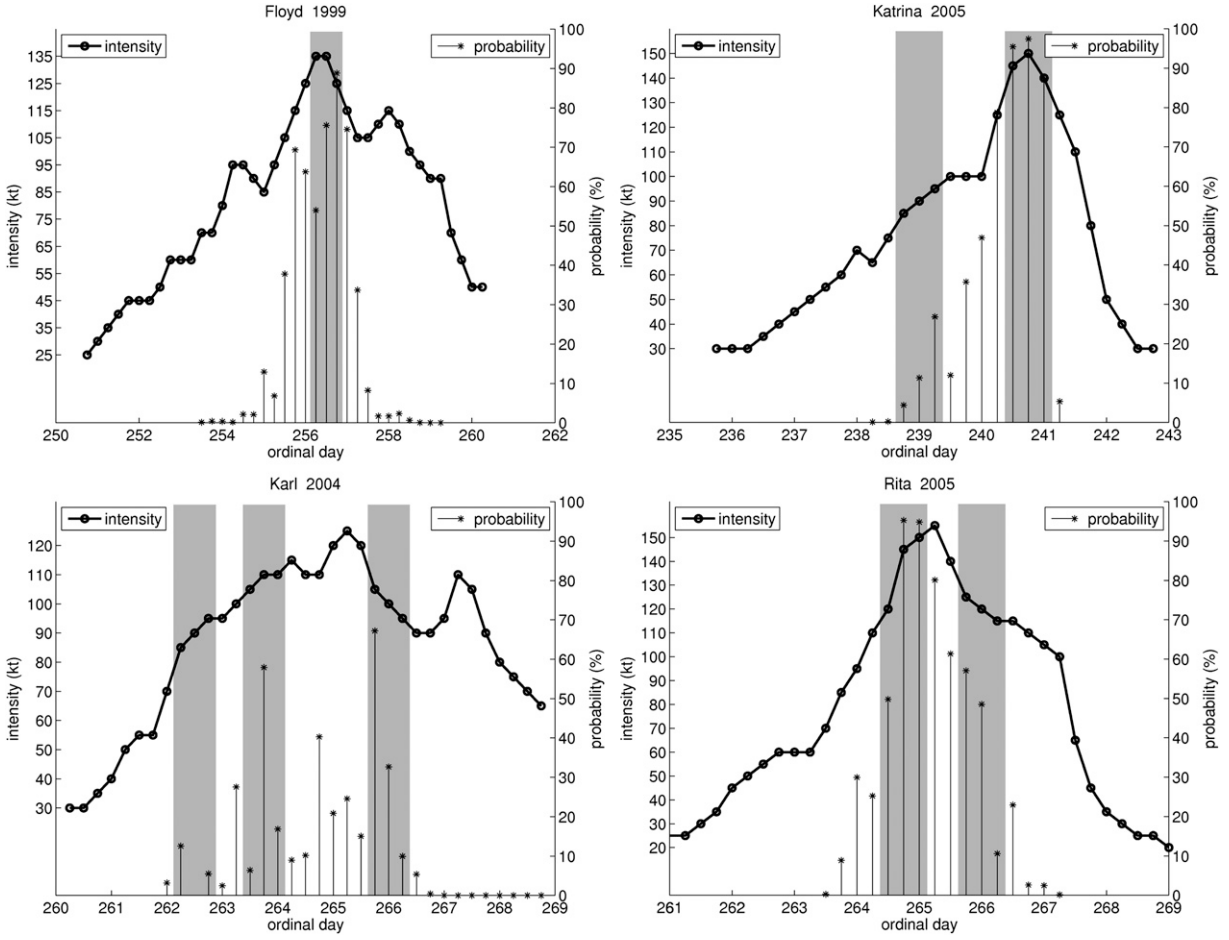

FIG. 9. Evolution of current intensity (solid black line, left axis) and model-estimated probability of secondary eyewall formation (stem plot, right axis) in Hurricanes Floyd (1999), Karl (2004), Katrina (2005), and Rita (2005). Each gray shaded region denotes a period that a secondary eyewall formation event was observed within. The model does not assign a probability when intensity is less than 65 kt (33 m s^{-1}) or when the storm center is over land.

significantly controlling the probabilities assigned by the model. For example, the probability in Hurricane Floyd (1999) remained fairly constant and close to zero during a prolonged intensification period and again for a period after maximum intensity but while the intensity was still high. Near-zero probabilities are also seen while Hurricane Karl (2004) was a major hurricane but was moving northward into an environment that was unfavorable for secondary eyewall formation.

b. Application to the central and eastern North Pacific

All procedures performed using the North Atlantic data were repeated for the central and eastern North Pacific. In general, secondary eyewall formation is less probable than in the North Atlantic, and consequently our sample size is smaller. Analogous to the procedure performed with the North Atlantic sample, the choice of

TABLE 7. SHIPS features applied to the Bayes probabilistic model in the central and eastern North Pacific.

SHIPS feature	Description	Preference
VMX	Current intensity	Stronger
TWXC	0–600-km maximum symmetric tangential wind at 850 hPa from NCEP analysis	Stronger
SHRD	850–200-hPa shear magnitude	Weaker
VMPI	Maximum potential intensity	Narrower, higher
IR00–10	Percent area between 50 and 200 km with GOES infrared brightness temperature colder than −50°C	Narrower range, colder

TABLE 8. Same as Table 3 but for the central and eastern North Pacific.

		Observed	
	Forecast	Yes	No
Climatology	Yes	0	0
	No	41	706
Current intensity only	Yes	0	2
	No	41	704
Current intensity plus	Yes	5	6
SHIPS environmental	No	36	700
Current intensity plus	Yes	10	10
SHIPS environmental plus GOES	No	31	696

features here was based on statistically significant separation by class, and performance of the model in cross-validation. In this case, the feature set applied in the central and eastern North Pacific comprises four storm/environmental features and one satellite-based feature from the SHIPS dataset (described in Table 7) plus the additional satellite-derived feature derived from the principal component analysis described in section 2. Similar to the results in the North Atlantic, secondary eyewall formation is associated with higher maximum potential intensity (VMPI) and lower vertical wind shear (SHRD), but the relationship with upper-level zonal wind and middle- to upper-level relative humidity is no longer evident. The differences in how the features contribute to the model skill in the central and eastern North Pacific compared to the North Atlantic are suggestive that the environmental control of secondary eyewall formation has different sensitivities in each basin.

The cross-validated model skill, as indicated by the Brier and Peirce skill scores, increases markedly with the inclusion of the environmental and satellite-derived features, although the model is less skillful than in the North Atlantic (Tables 8 and 9). When the Briggs and Ruppert skill score is considered, the model is found to have no skill in diagnosing secondary eyewall formation in the central and eastern North Pacific. Again, this emphasizes that skill scores with different sensitivities can vary greatly. In this case, the differences in skill scores are a likely indication that the model is comparatively not as robust when applied to central and eastern North Pacific hurricanes.

5. Summary

The purpose of this study was to assess the environmental conditions associated with secondary eyewall formation in hurricanes and to apply this information, combined with satellite-derived information, to the construction of an objective tool to provide probabilities of secondary eyewall formation in an operational setting. We formed a large database of secondary eyewall formation events in the North Atlantic and central and eastern North Pacific Oceans, and documented a climatology of secondary eyewall formation. We constructed composites of the ambient storm-centered environmental and satellite-derived fields for cases when a secondary eyewall formed in the following 12 h and for cases when no secondary eyewall formed in the following 12 h, and found significant differences between them. Some of these differences were due to differences in hurricane intensity, but we found that the environment plays a significant additional role in modulating secondary eyewall formation. We then exploited these differences using a naïve Bayes probabilistic model that provides an estimate of the probability of imminent secondary eyewall formation. In leave-one-year-out cross-validation over a 10-yr period, the model was shown to be skillful when measured against a climatology defined by event counts, although varying measures of model skill in the central and eastern Pacific were not as consistent as the North Atlantic. The methodology applied in this study to North Atlantic and central and eastern Pacific secondary eyewall formation is presently being repeated for western North Pacific tropical cyclones.

It is expected that the model described here will be combined with the annular hurricane index described by Knaff et al. (2003, 2008) to form a general objective tool that diagnoses imminent structure changes in hurricanes. Annular hurricanes describe a class of hurricanes that tend to have a single eyewall that is larger and more circularly symmetric than average. It is

TABLE 9. Performance metrics of the algorithm applied to the central and eastern North Pacific (cf. with Table 4 for the North Atlantic).

	Brier skill score	Peirce skill score	Briggs and Ruppert skill score	Probability of detection	False alarm rate	Area under ROC curve
Climatology	0%	0%	0%	0%	0%	0.50
Current intensity only	11%	0%	−5%	0%	0%	0.80
Current intensity plus SHIPS environmental	10%	11%	−2%	12%	1%	0.88
Current intensity plus SHIPS environmental plus GOES	13%	23%	0%	24%	1%	0.87

hypothesized that the precursor to annular hurricane formation is the formation of a secondary eyewall that does not contract to the size of the primary eyewall it surrounds, but instead reaches a quasi–steady state at a larger radius. Thus annular hurricane formation and eyewall replacement cycles might be viewed as similar phenomena that both begin with the formation of a secondary eyewall, but evolve somewhat differently after that. In this respect, secondary eyewall formation events form a crucial pathway to a broad range of hurricane structure changes, which directly modulate the threat to coastal communities and marine interests. This provides a strong motivation to increase both our physical understanding of these events and our ability to accurately diagnose and forecast them in an operational setting.

Acknowledgments. We thank Jeff Hawkins for providing an earlier version of his secondary eyewall database and for his assistance with the microwave imagery. The microwave imagery is provided by the Naval Research Laboratory in Monterey, California. We're grateful to Dave Nolan, Chris Rozoff, John Knaff, Mark DeMaria, and Chris Velden for many useful discussions; and to Howard Berger for his contributions to an earlier version of this work. We also thank Mark DeMaria for providing the SHIPS developmental dataset. This work is supported under the NOAA GOES-R Risk Reduction project and by the Office of Naval Research under Grant N00014-07-1-0163. Earlier work related to this project was funded by the NOAA Hurricane Supplemental Research Program and NRL-MRY Satellite Applications Grant N00173-01-C-2024.

REFERENCES

Bellman, R. E., 1957: *Dynamic Programming*. Princeton University Press, 342 pp.

Bishop, C. M., 1995: *Neural Networks for Pattern Recognition*. Oxford University Press, 482 pp.

Bister, M., and K. A. Emanuel, 1998: Dissipative heating and hurricane intensity. *Meteor. Atmos. Phys.,* **52,** 233–240.

Black, M. L., and H. E. Willoughby, 1992: The concentric eyewall cycle of Hurricane Gilbert. *Mon. Wea. Rev.,* **120,** 947–957.

Briggs, W., and D. Ruppert, 2005: Assessing the skill of yes/no predictions. *Biometrics,* **61,** 799–807.

——, M. Pocernich, and D. Ruppert, 2005: Incorporating misclassification error in skill assessment. *Mon. Wea. Rev.,* **133,** 3382–3392.

Camp, J. P., and M. T. Montgomery, 2001: Hurricane maximum intensity: Past and present. *Mon. Wea. Rev.,* **129,** 1704–1717.

DeMaria, M., and J. Kaplan, 1994: A Statistical Hurricane Intensity Prediction Scheme (SHIPS) for the Atlantic basin. *Wea. Forecasting,* **9,** 209–220.

——, and ——, 1999: An updated Statistical Hurricane Intensity Prediction Scheme (SHIPS) for the Atlantic and eastern North Pacific basins. *Wea. Forecasting,* **14,** 326–337.

——, M. Mainelli, L. K. Shay, J. A. Knaff, and J. Kaplan, 2005: Further improvements to the Statistical Hurricane Intensity Prediction Scheme (SHIPS). *Wea. Forecasting,* **20,** 531–543.

Dodge, P., R. W. Burpee, and F. D. Marks, 1999: The kinematic structure of a hurricane with sea level pressure less than 900 mb. *Mon. Wea. Rev.,* **127,** 987–1004.

Domingos, P., and M. Pazzani, 1997: Beyond independence: Conditions for the optimality of the simple Bayesian classifier. *Mach. Learn.,* **29,** 103–130.

Elsner, J., and C. Schmertmann, 1994: Assessing forecast skill through cross validation. *Wea. Forecasting,* **9,** 619–624.

Fortner, L. E., 1958: Typhoon Sarah, 1956. *Bull. Amer. Meteor. Soc.,* **39,** 633–639.

Hand, D. J., and K. Yu, 2001: Idiot's Bayes: Not so stupid after all? *Int. Stat. Rev.,* **69,** 385–398.

Hawkins, J. D., and M. Helveston, 2004: Tropical cyclone multiple eyewall characteristics. *Extended Abstracts, 26th Conf. on Hurricanes and Tropical Meteorology*, Miami, FL, Amer. Meteor. Soc., P1.7.

——, and Coauthors, 2006: Tropical cyclone multiple eyewall configurations. *Extended Abstracts, 27th Conf. on Hurricanes and Tropical Meteorology*, Monterey, CA, Amer. Meteor. Soc., 6B.1.

Houze, R. A., Jr., S. S. Chen, B. F. Smull, W.-C. Lee, and M. M. Bell, 2007: Hurricane intensity and eyewall replacement. *Science,* **315,** 1235–1239.

Knaff, J. A., J. P. Kossin, and M. DeMaria, 2003: Annular hurricanes. *Wea. Forecasting,* **18,** 204–223.

——, T. A. Cram, A. B. Schumacher, J. P. Kossin, and M. DeMaria, 2008: Objective identification of annular hurricanes. *Wea. Forecasting,* **23,** 17–28.

Knapp, K. R., and J. P. Kossin, 2007: A new global tropical cyclone data set from ISCCP B1 geostationary satellite observations. *J. Appl. Remote Sensing,* **1,** 013505, doi:10.1117/12.731296.

Kossin, J. P., W. H. Schubert, and M. T. Montgomery, 2000: Unstable interactions between a hurricane's primary eyewall and a secondary ring of enhanced vorticity. *J. Atmos. Sci.,* **57,** 3893–3917.

——, K. R. Knapp, D. J. Vimont, R. J. Murnane, and B. A. Harper, 2007a: A globally consistent reanalysis of hurricane variability and trends. *Geophys. Res. Lett.,* **34,** L04815, doi:10.1029/2006GL028836.

——, and Coauthors, 2007b: Estimating hurricane wind structure in the absence of aircraft reconnaissance. *Wea. Forecasting,* **22,** 89–101.

Kuo, H.-C., L.-Y. Lin, C.-P. Chang, and R. T. Williams, 2004: The formation of concentric vorticity structures in typhoons. *J. Atmos. Sci.,* **61,** 2722–2734.

Kwon, Y. C., and W. M. Frank, 2008: Dynamic instabilities of simulated hurricane-like vortices and their impacts on the core structure of hurricanesPart II: Moist experiments. *J. Atmos. Sci.,* **65,** 106–122.

Landsea, C. W., and Coauthors, 2004: A reanalysis of Hurricane Andrew's intensity. *Bull. Amer. Meteor. Soc.,* **85,** 1699–1712.

Molinari, J., and D. Vollaro, 1989: External influences on hurricane intensity. Part I: Outflow layer eddy angular momentum fluxes. *J. Atmos. Sci.,* **46,** 1093–1105.

Montgomery, M. T., and R. J. Kallenbach, 1997: A theory for vortex Rossby-waves and its application to spiral bands and intensity changes in hurricane. *Quart. J. Roy. Meteor. Soc.,* **123,** 435–465.

Nong, S., and K. A. Emanuel, 2003: A numerical study of the genesis of concentric eyewalls in hurricane. *Quart. J. Roy. Meteor. Soc.,* **129,** 3323–3338.

Ooyama, K., 1969: Numerical simulation of the life cycle of tropical cyclones. *J. Atmos. Sci.,* **26,** 3–40.

Rozoff, C. M., W. H. Schubert, B. D. McNoldy, and J. P. Kossin, 2006: Rapid filamentation zones in intense tropical cyclones. *J. Atmos. Sci.,* **63,** 325–340.

——, ——, and J. P. Kossin, 2008: Some dynamical aspects of tropical cyclone concentric eyewalls. *Quart. J. Roy. Meteor. Soc.,* **134,** 583–593.

Samsury, C. E., and E. J. Zipser, 1995: Secondary wind maxima in hurricanes: Airflow and relationship to rainbands. *Mon. Wea. Rev.,* **123,** 3502–3517.

Shapiro, L. J., and H. E. Willoughby, 1982: The response of balanced hurricanes to local sources of heat and momentum. *J. Atmos. Sci.,* **39,** 378–394.

Terwey, W. D., and M. T. Montgomery, 2006: Modeled secondary eyewall and spiral band dynamics. *Extended Abstracts, 27th Conf. on Hurricanes and Tropical Meteorology*, Monterey, CA, Amer. Meteor. Soc., 2B.3.

Wang, Y., 2008: Rapid filamentation zone in a numerically simulated tropical cyclone. *J. Atmos. Sci.,* **65,** 1158–1181.

Wilks, D. S., 2006: *Statistical Methods in the Atmospheric Sciences.* 2nd ed. International Geophysics Series, Vol. 91, Academic Press, 627 pp.

Willoughby, H. E., and P. G. Black, 1996: Hurricane Andrew in Florida: Dynamics of a disaster. *Bull. Amer. Meteor. Soc.,* **77,** 543–549.

——, J. A. Clos, and M. Shoreibah, 1982: Concentric eye walls, secondary wind maxima, and the evolution of the hurricane vortex. *J. Atmos. Sci.,* **39,** 395–411.

Wu, L., S. A. Braun, J. Halverson, and G. Heymsfield, 2006: A numerical study of Hurricane Erin (2001). Part I: Model verification and storm evolution. *J. Atmos. Sci.,* **63,** 65–86.

Zhang, H., 2006: On the optimality of naïve Bayes with dependent binary features. *Pattern Recog. Lett.,* **27,** 830–837.

Zhu, T., D. L. Zhang, and F. Weng, 2004: Numerical simulation of Hurricane Bonnie (1998). Part I: Eyewall evolution and intensity changes. *Mon. Wea. Rev.,* **132,** 225–241.